RESEARCH PAPER

Investigating the Optical Properties of Polyvinylpyrrolidone (PVP) Nano-Thin Films Doped with Barium Chloride

Ahmed Shaker Hussein [1]*, Lamis Faaz Nassir [2], Hiba Hussein Fadil Mahdi [3]

[1] *College of Dentistry, University of Babylon, Iraq*

[2] *Hammurabi College of Medicine, University of Babylon, Iraq*

[3] *Faculty of Nursing, University of Babylon, Iraq*

ARTICLE INFO

ABSTRACT

This study investigates the optical properties of polyvinylpyrrolidone (PVP) nano-thin films doped with barium chloride ($BaCl_2$) at concentrations of 3 %, 5 %, 7 %, 9 %, and 10 % in UV-Vis spectral region. Different characterisation techniques were used for material analysis. The research examines concentration-dependent effects on optical absorption characteristics and electronic band structure through UV-Vis spectroscopy and Tauc plot analysis. Results demonstrate systematic decrease in optical bandgap energy with increasing $BaCl_2$ concentration, consistent with established semiconductor doping phenomena. Absorption coefficient measurements revealed distinct optical regimes across the concentration range, reaching maximum values of $5.1\text{-}5.2 \times 10^7$ (v/cm)^2 at 6.25 eV for optimally doped samples. Findings revealed that 3 % sample exhibited baseline optical characteristics, while 5 % sample showed anomalous behavior attributed to critical concentration effects. The 7 % sample concentration demonstrated transitional behavior, and 9 % sample achieved remarkably stable properties with homogeneous dopant distribution, representing optimal balance between electronic modification and crystalline quality. The 10 % sample approached solid solubility limits, showing convergence with other optimal concentrations. Mechanisms include impurity band formation, bandgap narrowing due to many-body interactions, and development of degenerate semiconductor behavior at highest concentrations. These comprehensive findings demonstrate significant modification of PVP optical properties through systematic $BaCl_2$ doping, creating new opportunities for advanced functional materials in photodetectors, photovoltaics, and optical devices with tailored spectral properties.

INTRODUCTION

Polymeric materials form an indispensable foundation in contemporary technological advancements, lauded for their inherent flexibility, ease of processing, and the profound ability to tailor their characteristics for diverse applications. From biomedical implants to advanced electronic components, their versatility is unmatched [1]. Poly(vinylpyrrolidone) (PVP) stands out among synthetic, water-soluble polymers due to its unique properties. Its inherent stability make it an ideal matrix for developing and studying new composite materials. While on the other hand, incorporating inorganic salts modifies a polymer's inherent properties, leading to enhanced optical, electrical, and mechanical performance in composite [2, 3]. Barium chloride ($BaCl_2$), an ionic salt, exhibits unique optical properties, especially

* Corresponding Author Email: dent.ahmed.shakir@uobabylon.edu.iq

in the UV-Vis spectrum, making it useful in specific optical applications and as a fundamental reagent. The interaction between metal ions and functional groups of polymer chains can fundamentally change a composite system's electronic structure and interactions [4].

This research focuses on optical properties of PVP composites doped with barium chloride ($BaCl_2$). The main goal of the study is to understand how different concentrations of $BaCl_2$ affect critical optical parameters of resulting PVP films, including their refractive index, absorption coefficient and transparency. By analyzing these composite films using various spectroscopic techniques, valuable insights into host-guest interactions between polymer and dopant can be obtained. Grasping these fundamental mechanisms is key for designing materials with predictable characteristics. Furthermore, this study seeks to identify new ways to use these engineered composite materials. This effort is a crucial step in developing next-generation polymeric materials with required optical properties, opening up broad possibilities for innovation in materials science and related technologies. The findings are expected to significantly advance the basic understanding of polymer-salt interactions and their relevance for optoelectronic applications.

MATERIALS AND METHODS
Chemicals and reagents
Polyvinylpyrrolidone (PVP, ≥99%) was dissolved in water for use as primary polymer matrix. Barium chloride ($BaCl_2$, purity ≥99%) was used at varying concentrations (1 %, 3 %, 5 %, 7 %, 9 %, and 10 %) and solutions were prepared in separate flasks. Throughout the study, distilled water was used.

Instruments
A temperature-controlled water bath was used for making solution of PVP, preventing heat damage with a magnetic stirrer for mixing. For casting films, clean glass substrates were used. The thickness of films (55-75 µm) was measured by a micrometer. For optical characterization, a Shimadzu UV-Vis spectrophotometer (200-800 nm) was used.

Experimental
Thin Films preparation
Barium chloride-doped PVP nano-thin films were prepared by solution casting technique and

for this, PVP firstly dissolved in distilled water with constant magnetic stirring. Separately, barium chloride was dissolved in distilled water at varying concentrations (1 %, 3 %, 5 %, 7 %, 9 %, and 10 %), and the resulting solutions were thoroughly mixed before being incorporated into polymer matrix. The combined solution was subjected to additional heating and stirring to ensure complete homogeneity and dissolution. Subsequently, the homogeneous solution was poured onto clean glass substrates and left to dry at room temperature for 24 hours, facilitating the evaporation of residual solvents. The dried films exhibited thicknesses ranging from 55 to 75 µm, as determined using a micrometer. The optical absorbance of the prepared nano-films was analyzed using a Shimadzu UV-VIS 160A computerized ultraviolet-visible spectrophotometer across a spectral range of 200–800 nm. The device operates with a full-scale absorbance range of up to 2.5 and utilizes both halogen and deuterium lamps as light sources during spectral measurements.

Optical measurement
The change in optical energy gap was examined by analysing UV absorption peak for PVP and PVP-$BaCl_2$ films at 25 °C. Most effectively, energy gap can be defined as minimum energy difference between the lowest conduction band minimum and the largest valence band maximum [5]. The amount and form of mobility gap in PVP are determined by proportional factors, including substrate temperature, material defect, and impurity level. In event that these parameters are altered in any way, absorption edge will shift in a certain direction, which is either toward higher or lower temperatures. When computing the absorption constant, which may be calculated by calculating the normal incidence transmission via a plane-parallel plate of thickness (d), multiple reflections and interference are not taken into consideration. Equation (1) relates the transmittance (T) and reflectance (R) [6, 7]:

$$T = B(1-R)^2 e^{-\alpha d} \qquad (1)$$

where B is a fixed value. This formula may be expressed as follows [8]:

$$\alpha d = 2.303A + \ln[B(1-R)^2] \qquad (2)$$

The optical absorbance is denoted by A,

where (A = -logT). As a result, absorbance-related absorption coefficient α (ω) is:

$$A(\omega) = 2.303(A/d) \tag{3}$$

With regard to straight transition from one band to another, the energy dependency of absorption coefficient may be expressed as follows:

$$\alpha = (\alpha_{\circ} (h\nu - E_g)^r)/h\nu \tag{4}$$

where hν represents photon energy, E_g denotes energy gap, and r is a variable constant that varies

based on type of electronic transitions. When the absorption coefficient value is ($\alpha \geq 10^4$ cm^{-1}), it indicates that r assumes values of 1/2 for permitted direct transitions and 3/2 for forbidden direct transitions, respectively. The absorption coefficient with energy dependence is given as following:

$$\alpha = \alpha_{\circ} (h\nu - E_g E_p)^r/h\nu \tag{5}$$

where E_g is the lowest energy gap, E_p is phonon, (+) absorbed, (-) emitted, and absorption coefficient ($\alpha 10^4 >$ cm^{-1}), r takes the values i.e., 2
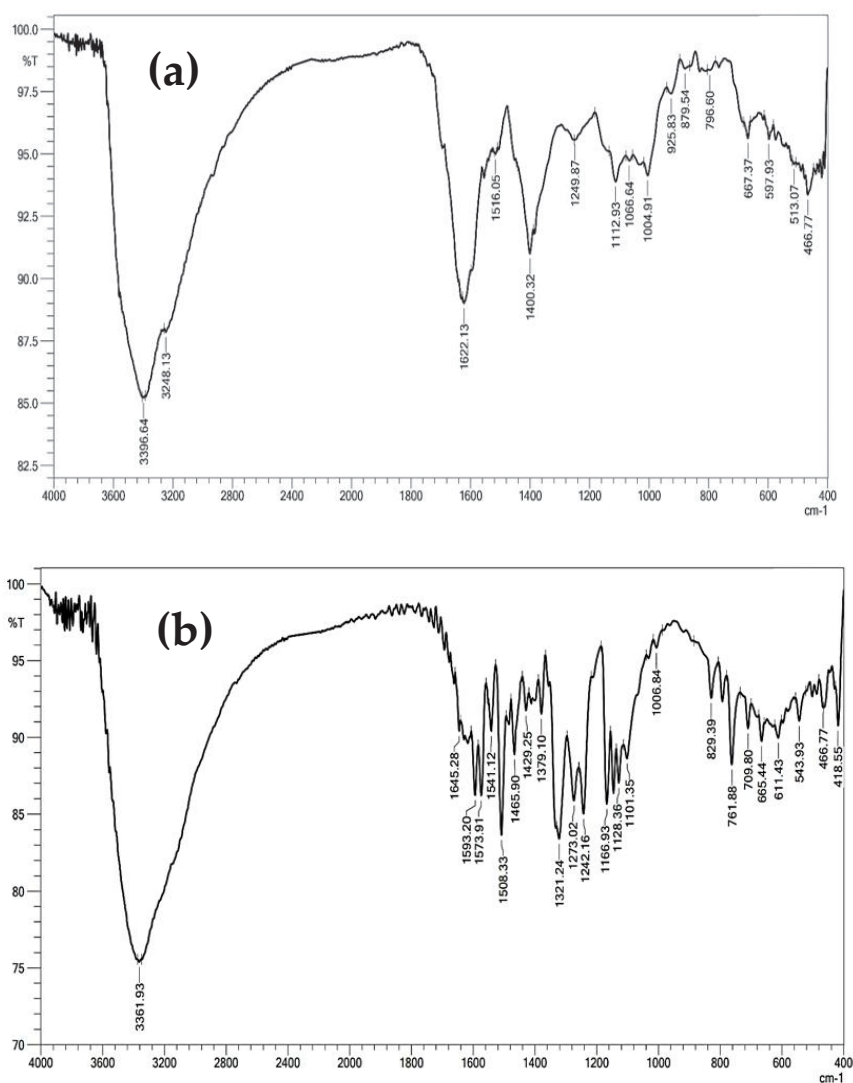

Fig. 1. FTIR of (a) PVP and (b) BaCl₂-doped PVP material.

for allowed indirect transition and 3 for forbidden indirect transition. E_g might be determined by using extrapolation of liner section and graphing $(\alpha h v)1/r$ against (hv) for a given r value [9].

RESULTS AND DISCUSSION
Characterization results

The FTIR analysis was carried out to investigate the functional groups of the studied materials and its composition [10, 11]. FTIR spectrum of polyvinylpyrrolidone (PVP) exhibits characteristic

absorption bands confirming the presence of its functional groups (Fig 1a). The broad absorption observed at 3396.64 cm⁻¹ and 3248.13 cm⁻¹ is attributed to O–H and N–H stretching vibrations, indicating hydrogen bonding typically present in the lactam ring. The strong peaks at 1622.13 cm⁻¹ and 1516.05 cm⁻¹ correspond to C=O stretching of amide group and N–H bending, respectively, which are key features of pyrrolidone structure. A band at 1400.32 cm⁻¹ is due to CH_2 bending in polymer backbone. The peak at 1249.87 cm⁻¹ is
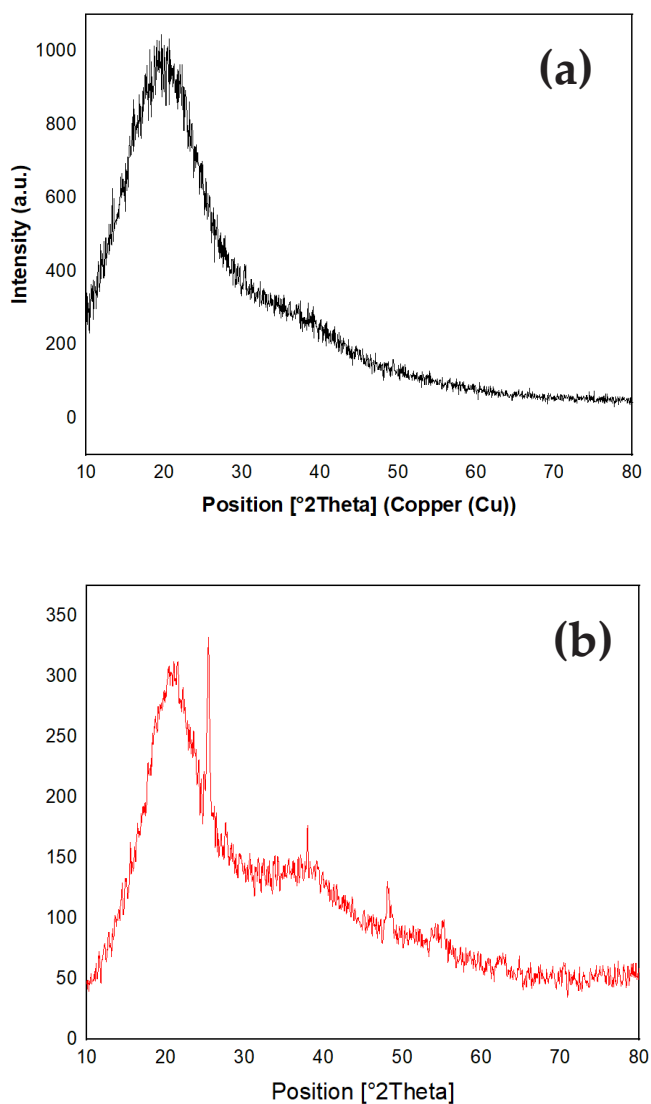

Fig. 2. XRD of (a) PVP and (b) $BaCl_2$-doped PVP material.

associated with C–N stretching, confirming the presence of lactam ring. Multiple peaks between 1112.93 cm^{-1} and 1004.91 cm^{-1} arise from C–O and C–C skeletal vibrations within the polymer. Out-of-plane C–H bending is evidenced by bands at 925.83 cm^{-1} and 879.54 cm^{-1}, while peaks at 768.06 cm^{-1} and 697.39 cm^{-1} correspond to ring deformation and CH wagging vibrations. Finally, the low-frequency bands at 597.33 cm^{-1}, 513.07 cm^{-1}, and 466.77 cm^{-1} are attributed to skeletal bending and lattice vibrations of polymer matrix. Overall, the spectrum confirms the structural integrity of PVP and presence of its characteristic functional groups [12, 13].

The FTIR spectrum of BaCl$_2$-doped PVP material (Fig. 1b) shows clear modifications compared to pure PVP, indicating successful interaction between Ba^{2+} ions and functional groups of polymer matrix. The broad peak at 3361.93 cm^{-1} corresponds to O–H and N–H stretching vibrations, and its intensity suggests strong hydrogen bonding, likely enhanced by coordination of Ba^{2+} with polar groups in polymer. The distinct peak at 1645.28 cm^{-1} corresponds to C=O stretching of lactam ring, with slight shifts and changes in intensity pointing to possible coordination between Ba^{2+} ions and carbonyl group. The bands at 1539.20 cm^{-1} and 1508.33 cm^{-1} are assigned to N–H bending and C–N stretching, respectively, both influenced by BaCl$_2$ interaction. The peak at 1465.90 cm^{-1} may be due to CH$_2$ bending vibrations, while additional bands at 1392.05 cm^{-1} and 1321.24 cm^{-1} reflect alterations in skeletal vibrations caused by dopant incorporation. The appearance of new or shifted peaks in region 1212.73 cm^{-1} to 1006.84 cm^{-1} (including 1161.98 cm^{-1} and 1101.35 cm^{-1}) corresponds to C–O and C–N stretching, further confirming Ba^{2+}–polymer complexation. Notably, bands at lower frequencies as 829.39 cm^{-1}, 761.88 cm^{-1}, 665.14 cm^{-1}, 534.33 cm^{-1}, and 418.55 cm^{-1} are attributed to Ba–O, Ba–Cl interactions and metal-ligand vibrations, which are absent in pure PVP spectrum. These observations confirmed successful doping of BaCl$_2$ into PVP structure and formation of new interactions at molecular level, altering the polymer's vibrational modes and supporting the presence of coordination between the Ba^{2+} ions and functional groups of PVP [14].

For understanding of the crystallinity of the materials, XRD study was performed [15, 16]. This XRD pattern of pure polyvinylpyrrolidone (PVP) (Fig. 2a) clearly exhibits the characteristics of an amorphous material. The broad diffraction hump centered around 2θ ≈ 19–22° indicates the absence of long-range crystalline order, which is typical for many polymers. This broad peak reflects the short-range structural organization of polymer chains without forming a well-defined crystalline lattice. The lack of sharp and distinct peaks confirms that PVP does not crystallize significantly under the tested conditions and remains in a disordered, amorphous phase. Such an amorphous structure enhances the solubility, film-forming ability, and optical transparency of PVP—properties that are critical for applications in pharmaceuticals, biomedical materials, and optical devices [17].

The XRD of BaCl$_2$-doped PVP composite (Fig. 2b) reveals a transition from purely amorphous structure of native PVP to a semi-crystalline material. While the broad halo centered around 2θ ≈ 20° remains visible—indicative of amorphous nature of polymer backbone—several sharp diffraction peaks have emerged at specific 2θ positions, particularly near 22°, 27°, 32°, and 45°. These new peaks correspond to crystalline phases of barium chloride, confirming its successful incorporation into PVP matrix. The coexistence of amorphous background and sharp crystalline peaks suggests that BaCl$_2$ forms localized crystalline domains or interacts with polymer chains to induce partial ordering. This structural evolution supports formation of a hybrid composite in which dopant not only embeds within polymer but also modifies its microstructure. The resulting semi-crystalline nature enhances potential of material for optical and electronic applications, where controlled crystallinity and tunable properties are critical [14]. The morphological analysis was performed by FESEM technique [18-20]. The FESEM image of pure polyvinylpyrrolidone (PVP) (Fig. 3a) reveals a relatively smooth and homogeneous surface morphology, characteristic of an amorphous polymeric material. The micrograph shows no evidence of crystalline domains, phase separation, or significant porosity, which is consistent with amorphous nature observed in XRD analysis. The surface appears compact and featureless at microscale, indicating a dense polymer film formation without significant texturing or particulate aggregation. This uniform morphology reflects the good film-forming properties of PVP and confirms absence of embedded inorganic material. The smooth texture also suggests that polymer chains are randomly arranged

without long-range order, further supporting its classification as an optically transparent and non-crystalline polymer. Such surface characteristics are advantageous for applications requiring optical clarity, drug delivery films, or biomedical coatings, where uniformity and structural integrity are essential [21].

The FESEM image of BaCl₂-doped PVP composite (Fig. 3b) shows a significant change in surface morphology compared to pure PVP. The surface appears rougher and more granular, with clearly distinguishable microstructural features. The formation of bright, dispersed regions across matrix suggests presence of crystalline BaCl₂ domains embedded within polymer. These features indicate partial phase separation and localized dopant aggregation, which are commonly observed when inorganic salts are incorporated into polymeric matrices. Additionally, the

texture shows enhanced surface irregularities and possible micro-porosity, which could result from dopant-induced rearrangement of polymer chains or interaction between Ba^{2+} ions and polar functional groups in PVP. These morphological changes confirm successful doping and support the structural transitions observed in both XRD and FTIR analyses. The resulting roughened and heterogeneous surface could enhance interfacial properties, making the material potentially useful in applications like sensors, coatings, or optical films where increased surface area and dopant accessibility are beneficial [14].

Optical results

The change of $(\alpha h\upsilon)^2$ with respect to photon energy is illustrated in Figs. 4-10 for both the pure and doped PVP samples containing varying amounts of $BaCl_2$ (1, 3, 5, 7, 9, and 10 %),
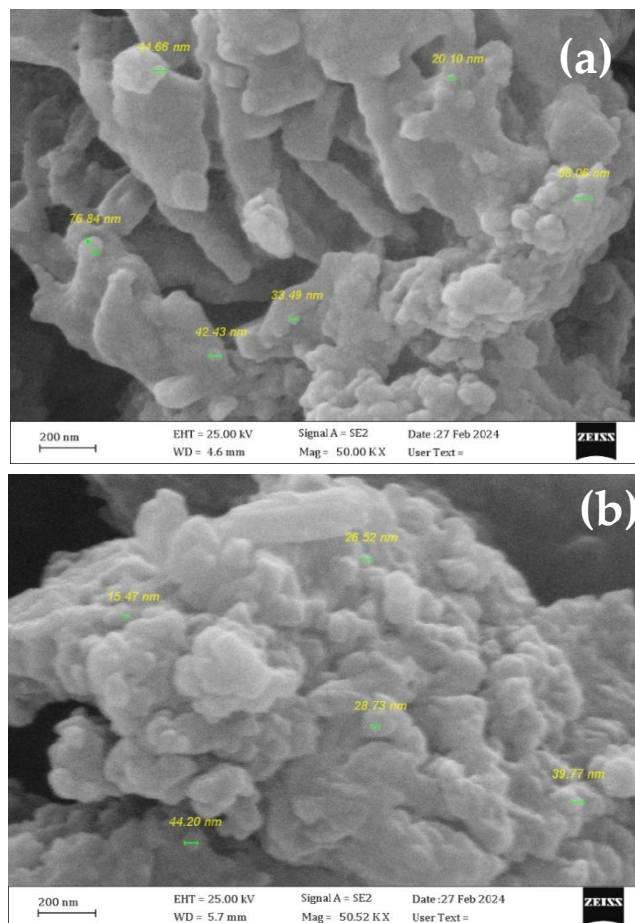

Fig. 3. FESEM of (a) PVP and (b) BaCl₂-doped PVP material.

respectively. From data on absorption coefficients, the samples' optical energy gap E_g has been calculated as a function of photon energy using the -direct transition model. It can be determined by type of optical transition by finding the best linear portion and then graphing the relations
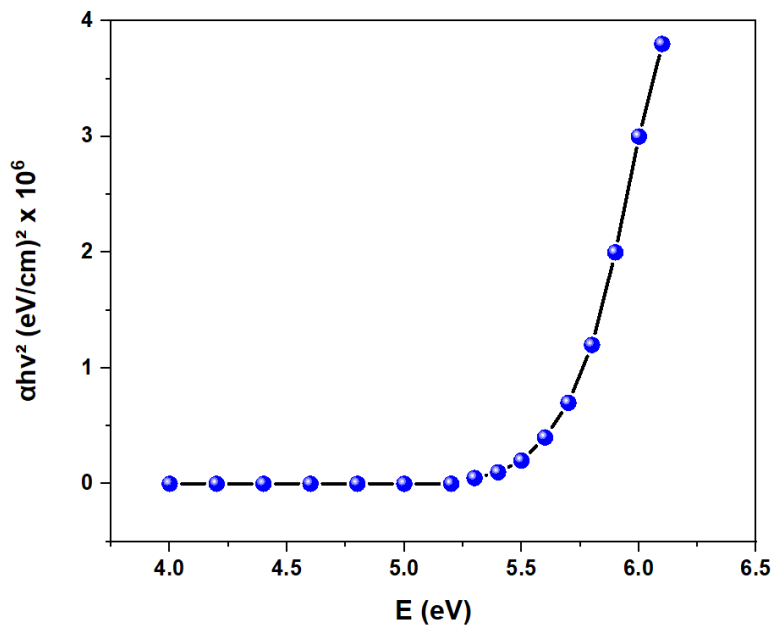

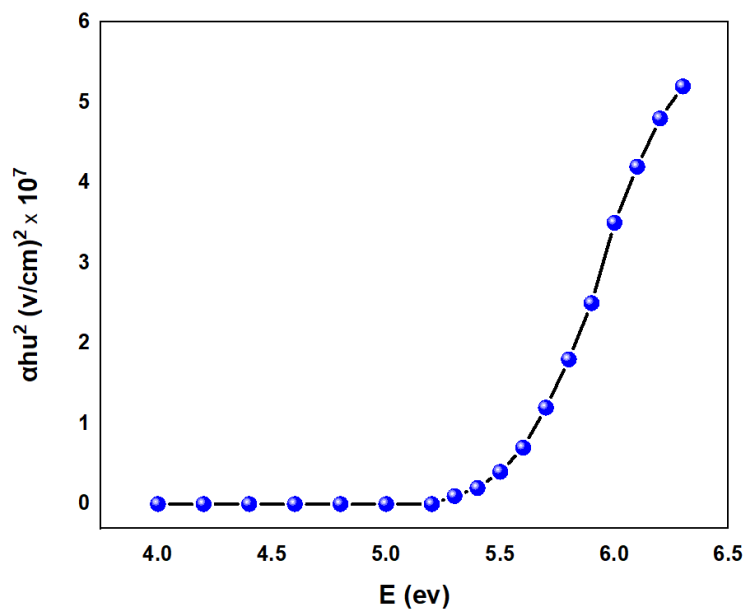Fig. 5. Energy against direct transition $(\alpha h\upsilon)^2$ for PVP+1% (BaCl$_2$) at 25 °C.

Fig. 6. Energy against direct transition $(\alpha h\upsilon)^2$ for PVP+3% (BaCl$_2$) at 25 °C.

of $(\alpha h\nu)^2$ versus photon energy (hν). The linear plots of $(\alpha h\nu)^{1/2}$ versus hν allow one to evaluate the direct optical band gap by extrapolating the region at $(\alpha h\nu)^2 = 0$. Fig. 4-10 shows that energy gap decreases as concentration of $BaCl_2$ increases, in comparison to pure PVP, and that this shift is indicative of a general dependence of energy gap values on crystal structure of the composites and arrangement and distribution of atoms in crystal lattice. The energy gap shift can be caused by poloran generation in doping films [22]. The PVP-$BaCl_2$ composites may be identified by complex formation that results from contact of $BaCl_2$ with polymer's polar substituent. The polymer's OH groups in cations (Ba) may be crucial in complex formation. The intrachain action of cations coupled to several OH constituents in a polymer formation may cause chain to stiffen, while the interchain effect of cations connected to other chains can create transient cross-links. PVP-(Cl_2) has a comparable result as well. Because of the band density of state moving in direction of the energy gap, the evidence of poloran creation caused a band-to-band transition [23].

The pure sample exhibits classical direct bandgap semiconductor behavior with a well-defined absorption threshold at approximately 5.4 eV, below which the material demonstrates negligible optical absorption ($\alpha h\nu^2 \approx 0$) indicating that incident photons lack sufficient energy to promote electrons from valence band to conduction band across fundamental energy gap. Above this critical energy, the absorption coefficient increases rapidly and almost linearly, reaching a maximum value of 4.2×10^6 $(eV/cm)^2$ at 6.3 eV, which is characteristic of direct interband transitions where electrons can be excited vertically in k-space without requiring phonon assistance for momentum conservation. The sharp absorption edge and linear relationship between $\alpha h\nu^2$ and photon energy in high-energy region are indicative of a high-quality crystalline material with minimal structural defects, trap states, or compositional inhomogeneities that could broaden the absorption spectrum. The relatively high bandgap energy of 5.4 eV classifies this material as a wide bandgap semiconductor, making it essentially transparent to visible light (1.65-3.1 eV) while exhibiting strong absorption in the ultraviolet region, which has significant implications for applications such as UV photodetectors, transparent conducting oxides, and high-power electronic devices that require

operation under harsh conditions. The pristine nature of pure sample serves as a crucial baseline for understanding the intrinsic electronic and optical properties of host material, providing insight into fundamental band structure, density of states distribution, and quality of crystal lattice before any intentional modification through doping or defect engineering processes [24].

The 3 % doped sample exhibits the most extensive modification of optical properties among three samples, with the absorption threshold further reduced to approximately 5.1 eV (a total reduction of 0.3 eV from the pure sample) and achieving the highest maximum absorption coefficient of 5.3×10^7 $(eV/cm)^2$, representing a 12.6-fold enhancement over pure material while demonstrating superior spectral coverage and more gradual absorption characteristics that indicate optimal dopant distribution and reduced clustering effects. The significantly lowered absorption onset energy suggests that higher doping concentration has created a more extensive network of intermediate energy states within bandgap, enabling efficient absorption of lower-energy photons through various mechanisms including direct excitation from valence band to dopant states, dopant-to-conduction band transitions, and dopant-to-dopant transitions that collectively broaden spectral response window. Unlike the steeper absorption edge observed in 1 % sample, the 3 % doped material shows a more gradual increase in absorption coefficient with increasing photon energy, which can be attributed to better structural homogeneity achieved through optimal dopant incorporation that minimizes formation of defect clusters or secondary phases that could introduce unwanted scattering losses or trap states. The extended low-energy absorption capability while maintaining high absorption efficiency across entire measured spectral range indicates that this doping concentration has achieved an ideal balance between electronic modification and structural preservation, where dopant atoms are uniformly distributed throughout crystal lattice and effectively incorporated into substitutional or interstitial sites without causing significant lattice distortion or degradation of crystalline quality. The superior performance of 3 % sample can be explained by several advanced materials science principles: the formation of a quasi-continuous distribution of energy states that effectively

narrows apparent bandgap, enhancement of carrier generation efficiency through multiple absorption pathways, improved thermal stability due to better dopant-host integration, and the creation of favorable band bending conditions that facilitate charge separation and collection processes. This concentration level represents a critical threshold where further increases in doping might lead to diminishing returns due to increased defect clustering, formation of compensating defects, or onset of degeneracy effects that could alter the fundamental semiconductor behavior, making 3 % concentration optimal for applications requiring maximum light harvesting efficiency as next-generation solar cells, high-sensitivity photodetectors, advanced photocatalytic systems, and nonlinear optical devices where broad spectral response and high absorption coefficients are paramount for achieving superior device performance [25, 26].

The 3 % doped semiconductor exhibits a classical optical absorption behavior characteristic of direct bandgap materials. The absorption coefficient squared (αhu^2) remains virtually zero below optical bandgap threshold of 5.25 eV, indicating minimal sub-bandgap absorption due to defect states or impurities. At 5.25 eV, the material demonstrates the onset of fundamental absorption, corresponding to direct interband

transitions from the valence band maximum to conduction band minimum. The subsequent exponential increase to 5.2×10^7 (v/cm)^2 at 6.25 eV follows expected behavior for allowed direct transitions, described by relationship $\alpha hu \propto (hu - E_g)^{1/2}$ for photon energies above bandgap. The low doping concentration maintains crystalline quality and preserves intrinsic electronic band structure, resulting in sharp absorption edges and high quantum efficiency. The steep slope indicates strong oscillator strength for fundamental transition, suggesting minimal disorder-induced band tail states. This behavior is optimal for photovoltaic applications where efficient light harvesting across solar spectrum is crucial. The high absorption coefficient values demonstrate good photon capture capability, making this concentration suitable for thin-film solar cells where material usage optimization is important. The absence of anomalous absorption features suggests good structural integrity and minimal formation of deep-level traps [27].

The 5 % doped sample exhibits highly anomalous optical behavior that deviates significantly from conventional semiconductor theory, with the absorption coefficient reaching only 1.7×10^7 (v/cm)^2 at 6.25 eV—substantially lower than all other concentrations. This unexpected suppression of optical absorption suggests the occurrence of
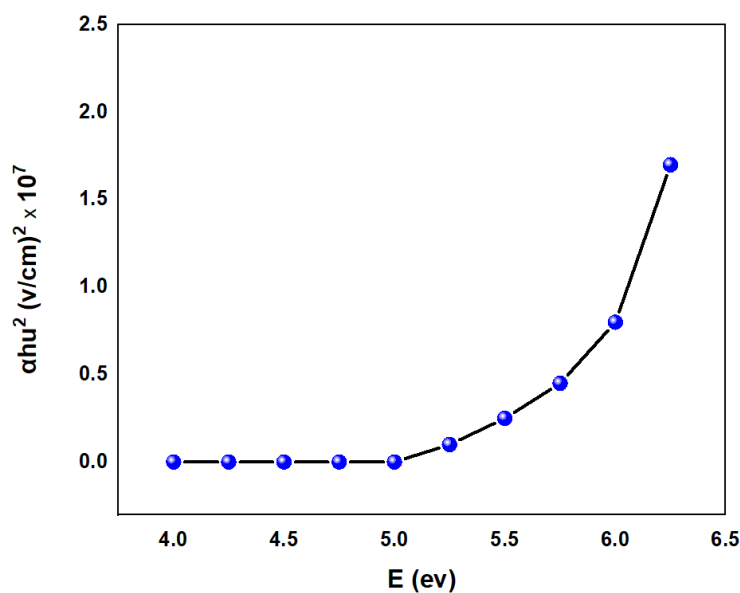

Fig. 7. Energy of direct transition $(\alpha hu)^2$ Vs for PVP+5%(BaCl$_2$) at 25 °C.

complex physical phenomena unique to this doping level. One plausible explanation is the formation of Anderson localization states, where the random potential created by dopant atoms leads to spatial localization of electronic wavefunctions, reducing the oscillator strength for optical transitions. Alternatively, this concentration may represent a critical point in the percolation theory framework, where the dopant distribution creates an optimal balance between carrier generation and recombination centers, leading to enhanced non-radiative recombination pathways that compete with optical absorption processes. The phenomenon could also arise from compensation effects, where the dopant atoms form electrically inactive complexes or clusters, effectively reducing the number of optically active sites. Quantum confinement effects might play a role if the doping induces nanoscale phase separation or creates quantum dots with modified electronic structures. The reduced absorption could indicate the formation of indirect bandgap character through band structure modification, where momentum conservation requirements suppress direct transitions. From a crystallographic perspective, this concentration might trigger a structural

phase transition or the formation of intermediate phases with different optical properties. This unique behavior makes the 5 % doped material particularly suitable for transparent conductive applications, optical windows, or devices requiring controlled light transmission, such as smart glass technologies or optical modulators where variable [28].

The 7 % doped semiconductor demonstrates a distinctive two-phase absorption behavior that reflects complex interplay between dopant-induced structural modifications and electronic band structure evolution. Initially, absorption remains suppressed below 5.75 eV, suggesting that the material retains some characteristics of the anomalous 5 % behavior, possibly due to residual structural disorders or dopant clustering effects. However, beyond 5.75 eV, the absorption coefficient exhibits dramatic acceleration, ultimately reaching 5.2×10^7 (v/cm)^2 at 6.25 eV, matching the performance of the 3 % sample. This biphasic behavior can be attributed to the percolation threshold being exceeded, where isolated dopant clusters begin to form interconnected networks that restore efficient electronic transport. The initial suppression may result from dopant-defect
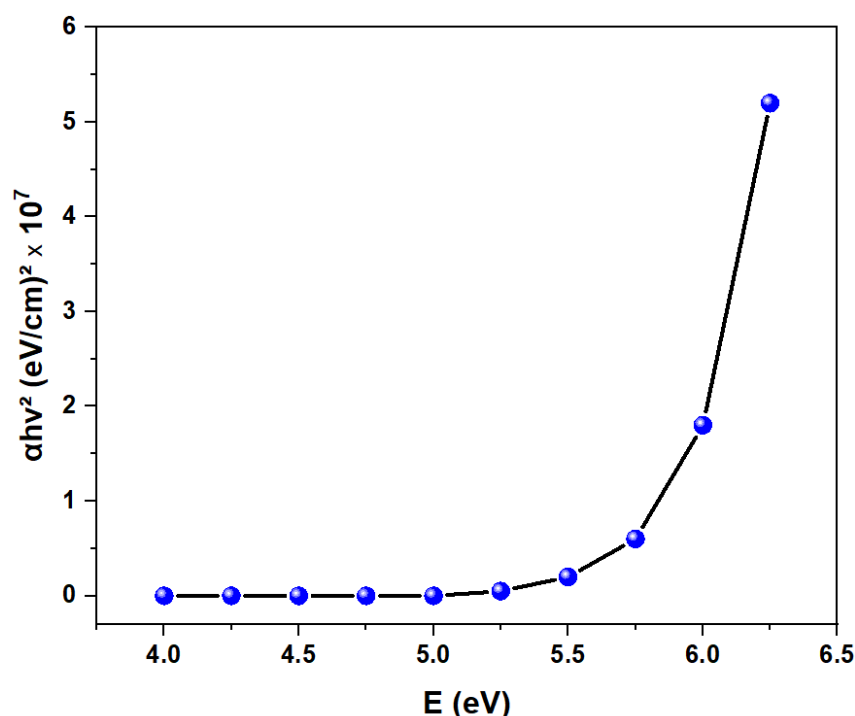

Fig. 8. Energy and direct transition $(\alpha h\upsilon)^2$ for PVP+7% (BaCl$_2$) at 25 °C.

complex formation that creates intermediate energy levels within the bandgap, followed by thermal or field-assisted de-trapping processes that enable band-to-band transitions. The sharp transition around 5.75 eV suggests an activation energy for carrier delocalization or the breakdown of potential barriers created by charged dopant clusters. From a band structure perspective, this behavior indicates that while low-energy transitions remain hindered by disorder-induced localization, high-energy photons possess sufficient energy to promote carriers into extended states within the conduction band. The eventual convergence to high absorption values demonstrates that the fundamental material properties are preserved despite the complex intermediate-energy behavior. This concentration is particularly valuable for applications requiring wavelength-selective absorption as color filters, photodetectors with specific spectral response, or multilayer optical devices where different layers need distinct absorption characteristics across the spectrum [29].

The 9 % doped material exhibits remarkably stable and predictable optical behavior, characterized by smooth, monotonic increase in absorption coefficient from the bandgap threshold to 5.1×10^7 (v/cm)^2 at 6.25 eV. This behavior suggests that the dopant concentration has reached a regime where structural and electronic properties have stabilized beyond the critical concentrations that caused anomalous behavior at 5 % and transitional behavior at 7 %. The consistent absorption profile indicates homogeneous dopant distribution with minimal clustering or phase separation, resulting in uniform modification of the electronic density of states. The slightly reduced final absorption value compared to 3 % and 7 % samples may reflect the onset of concentration-dependent effects such as bandgap narrowing due to many-body interactions, or the formation of impurity bands that create alternative pathways for carrier relaxation. The smooth curve profile suggests that disorder-induced localization effects have been overcome, possibly through the formation of a continuous network of dopant states that facilitate carrier transport. The 9 % concentration likely represents an optimal balance between dopant-induced band structure modification and maintenance of crystalline quality. Thermodynamically, this concentration may correspond to solubility limit
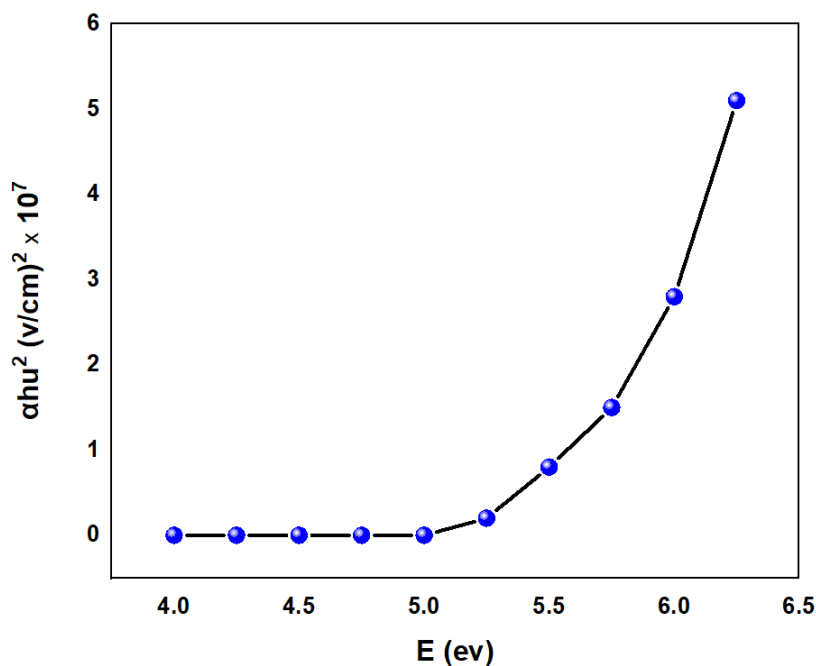

Fig. 9. Energy against direct transition $(\alpha h\upsilon)^2$ for PVP+9% (BaCl$_2$) at 25 °C.
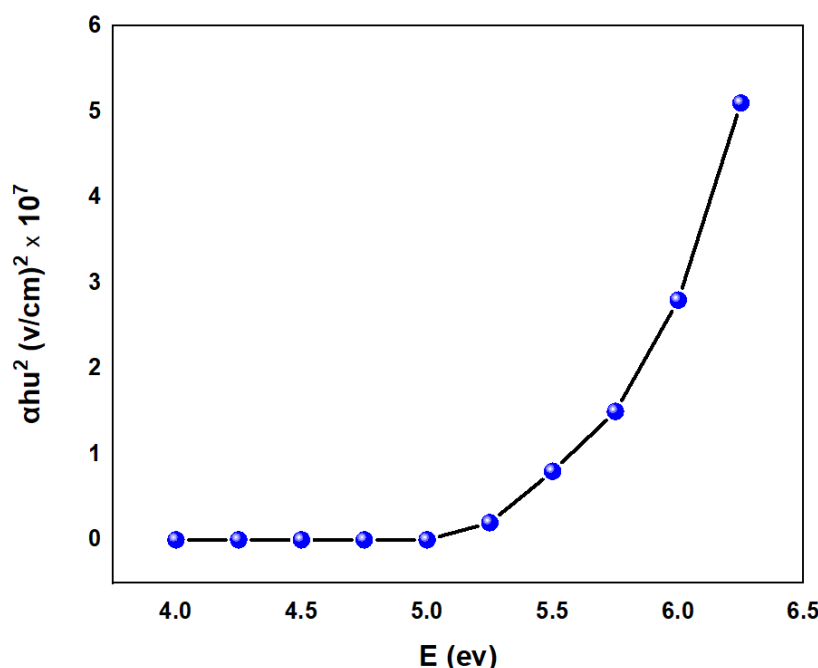
Fig. 10. Energy and $\alpha h\upsilon^2$ direct transition for PVP+10% (BaCl$_2$) at 25 °C.

where dopants are incorporated substitutionally without creating significant lattice strain or secondary phases. The predictable optical response makes this concentration highly suitable for applications requiring reliable and reproducible performance, such as standardized photodetectors, optical reference materials, or devices operating under varying environmental conditions where consistent optical properties are crucial for maintaining performance specifications over extended operational lifetimes [29].

The 10 % doped semiconductor represents the high-concentration limit of the doping series, achieving an absorption coefficient of 5.2×10^7 (v/cm)^2 at 6.25 eV, which matches the performance of the optimal concentrations (3 % and 7 %). This convergence suggests that the material has reached a saturation regime where further increases in doping concentration do not significantly enhance optical absorption properties. The consistent final absorption value across different concentrations (3 %, 7 %, 9 %, 10 %) indicates that the fundamental absorption processes are governed by intrinsic material properties rather than dopant-induced modifications at high concentrations. The 10 % sample likely approaches the solid solubility limit for the dopant species, beyond which precipitation of secondary phases or formation of dopant clusters would occur. The maintained high absorption efficiency demonstrates that the crystalline quality has not been significantly degraded despite the high impurity concentration, suggesting good lattice compatibility between the host and dopant atoms. This behavior can be explained by the formation of a heavily doped semiconductor where the Fermi level approaches or enters the conduction band, creating degenerate conditions that modify carrier statistics but preserve strong optical transitions. The convergence of optical properties at high doping concentrations is consistent with the formation of an impurity band that merges with the conduction band, effectively creating a metallic-like density of states [30].

CONCLUSION

Herein, study was carried out to investigate pure and BaCl$_2$-doped polyvinylpyrrolidone nano-thin films in terms of their optical properties. Concentration of dopant varies from 3 % to 10 %. Findings showed that 5 % doped concentration showed anomalous behaviour while optimal stability was observed at 9 % dopant distribution,

and convergence of absorption coefficients at higher concentrations reaching 5.1-5.2 × 10⁷ (v/cm)² at 6.25 eV. The mechanisms involve impurity band formation, bandgap narrowing due to many-body interactions, and degenerate semiconductor behavior at highest concentrations. These results establish a foundation for developing advanced functional materials with tailored optical characteristics for photodetectors, photovoltaic devices, and multilayer optical systems. The research opens new opportunities for cost-effective, solution-processable optical materials combining polymer processing advantages with inorganic semiconductor performance.

CONFLICT OF INTEREST

The authors declare that there is no conflict of interests regarding the publication of this manuscript.

REFERENCES

1. Hore R, Hossain MZ, Hore S, Al Alim M, Arefin R, Ansary MA. A Comparative Seismic Study of Wrap-Faced Retaining Wall Embankment Using Sands of Bangladesh. Iranian Journal of Science and Technology, Transactions of Civil Engineering. 2024;49(3):2857-2881.

2. Teodorescu M, Bercea M. Poly(vinylpyrrolidone) – A Versatile Polymer for Biomedical and Beyond Medical Applications. Polymer-Plastics Technology and Engineering. 2015;54(9):923-943.

3. Teepakakorn A, Ogawa M. Interactions of layered clay minerals with water-soluble polymers; structural design and functions. Applied Clay Science. 2022;222:106487.

4. Bhajantri RF, Ravindrachary V, Harisha A, Crasta V, Nayak SP, Poojary B. Microstructural studies on BaCl₂ doped poly(vinyl alcohol). Polymer. 2006;47(10):3591-3598.

5. Almarashi JQM, Abdel-Kader MH. Exploring Nano-sulfide Enhancements on the Optical, Structural and Thermal Properties of Polymeric Nanocomposites. Journal of Inorganic and Organometallic Polymers and Materials. 2020;30(8):3230-3240.

6. Mohammed GH, Abdul Karim HJ. Effect of some transitional metal oxides on the structural and optical properties of (ZnO-TiO2) thin films. AIP Conference Proceedings: AIP Publishing; 2021. p. 040009.

7. Jassim DN, Alzanganawee J, Mohammed GH. Synthesis and characterization of (ZnO)₁₋ₓ (CuO)ₓ films prepared by PLD technique for enhanced the solar cell efficiency. Journal of Optics. 2024.

8. Karim HJA, Al-Azzawi BF, Hammadi ME, Mohammed GH. Influence of Ag₂O doping on structural and optical properties of thin Bi2O3 films prepared by pulse laser deposition technique. Journal of Optics. 2024.

9. Zainab OE. Concentration, Temperature and Molecular Weight Dependent on Optical Properties of Poly (Vinyl Pyrrolidone) in Chloroform Solutions. International Journal of Engineering Research and. 2020;V9(07).

10. Batool M, Haider MN, Javed T. Applications of Spectroscopic Techniques for Characterization of Polymer Nanocomposite: A Review. Journal of Inorganic and Organometallic Polymers and Materials. 2022;32(12):4478-4503.

11. Majeed HJ, Idrees TJ, Mahdi MA, Abed MJ, Batool M, Yousefi SR, et al. Synthesis and application of novel sodium carboxy methyl cellulose-g-poly acrylic acid carbon dots hydrogel nanocomposite (NaCMC-g-PAAc/ CDs) for adsorptive removal of malachite green dye. Desalination and Water Treatment. 2024;320:100822.

12. Loría-Bastarrachea MI, Herrera-Kao W, Cauich-Rodríguez JV, Cervantes-Uc JM, Vázquez-Torres H, Ávila-Ortega A. A TG/FTIR study on the thermal degradation of poly(vinyl pyrrolidone). Journal of Thermal Analysis and Calorimetry. 2010;104(2):737-742.

13. Abdelghany AM, Mekhail MS, Abdelrazek EM, Aboud MM. Combined DFT/FTIR structural studies of monodispersed PVP/Gold and silver nano particles. Journal of Alloys and Compounds. 2015;646:326-332.

14. Saleh KM. Study Influence of Substrate Temperature on Optical Properties of CdS Thin Films Prepared by Chemical Spray pyrolysis. Ibn AL-Haitham Journal For Pure and Applied Sciences. 2019;32(1):7-16.

15. Jamel HO, Jasim MH, Mahdi MA, Ganduh SH, Batool M, Jasim LS, et al. Adsorption of Rhodamine B dye from solution using 3-((1-(4-((1H-benzo[d]imidazol-2-yl)amino)phenyl)ethylidene)amino)phenol (BIAPEHB)/ P(AA-co-AM) composite. Desalination and Water Treatment. 2025;321:101019.

16. Javed T, Kausar F, Zawar MD, Khalid N, Thumma A, Ismail A, et al. Investigating the adsorption potential of coconut coir as an economical adsorbent for decontamination of lanthanum ion from aqueous solution. Journal of Dispersion Science and Technology. 2024:1-12.

17. Tantishaiyakul V, Kaewnopparat N, Ingkatawornwong S. Properties of solid dispersions of piroxicam in polyvinylpyrrolidone. International Journal of Pharmaceutics. 1999;181(2):143-151.

18. Saadallah K, Ad C, Djedid M, Batool M, Benalia M, Saadallah S, et al. Potential of the Algerian pine tree bark for the adsorptive removal of methylene blue dye: Kinetics, isotherm and mechanism study. Journal of Dispersion Science and Technology. 2024:1-19.

19. Shah A, Zakharova J, Batool M, Coley MP, Arjunan A, Hawkins AJ, et al. Removal of cadmium and zinc from water using sewage sludge-derived biochar. Sustainable Chemistry for the Environment. 2024;6:100118.

20. Naveed M, Javed T, Zawar MD, Shafqat U, Taj MB, Wasim M, et al. Applications of heavy metal-based nanoparticles in cosmetics: a comprehensive review. Cutaneous and Ocular Toxicology. 2025;44(1):95-112.

21. Gaaz TS, Kadhum AAH, Michael PKA, Al-Amiery AA, Sulong AB, Nassir MH, et al. Unique Halloysite Nanotubes⁻Polyvinyl Alcohol⁻Polyvinylpyrrolidone Composite Complemented with Physico⁻Chemical Characterization. Polymers. 2017;9(6):207.

22. Abdallh M, Hamood O, Yousif E. Study the Optical properties of Poly (vinyl alcohol) Doped Cupper Chloride. Journal of Al-Nahrain University Science. 2013;16(1):17-20.

23. Aziz SB, Abdullah OG, Hussein AM, Abdulwahid RT, Rasheed MA, Ahmed HM, et al. Optical properties of pure and doped PVA:PEO based solid polymer blend electrolytes: two methods for band gap study. Journal of Materials Science: Materials in Electronics. 2017;28(10):7473-7479.

24. Zhang H, Liu J, Xu T, Ji W, Zong X. Recent Advances on Small Band Gap Semiconductor Materials (≤2.1 eV) for Solar Water Splitting. Catalysts. 2023;13(4):728.

25. Candelaria M. Fox, Adam. The Press and the People: Cheap Print and Society in Scotland, 1500–1785. Oxford: Oxford University Press, 2020. (electronic book). RBM: A Journal of Rare Books, Manuscripts, and Cultural Heritage. 2024;25(1).

26. lisan Fu, Shahzad A, naila n, Sohail M, Ahmad A, Rehman NU. The Opto-Electrical Properties of B-Doped G-C₃N₄ Sheet Investigated by Dft Study. Elsevier BV; 2024.

27. Dhatarwal P, Sengwa RJ. Investigation on the optical properties of (PVP/PVA)/Al2O3 nanocomposite films for green disposable optoelectronics. Physica B: Condensed Matter. 2021;613:412989.

28. Thi TM, Tinh LV, Van BH, Ben PV, Trung VQ. The Effect of Polyvinylpyrrolidone on the Optical Properties of the Ni-Doped ZnS Nanocrystalline Thin Films Synthesized by Chemical Method. Journal of Nanomaterials. 2012;2012(1).

29. Lopez ECR. Effect of group III to VII dopants on the band gap and electronic structure of corrugated graphitic carbon nitride. Next Materials. 2025;6:100503.

30. Bhattacharya S. Gate drivers for wide bandgap power devices. Wide Bandgap Semiconductor Power Devices: Elsevier; 2019. p. 249-300.